Nanoscale

Accepted Manuscript

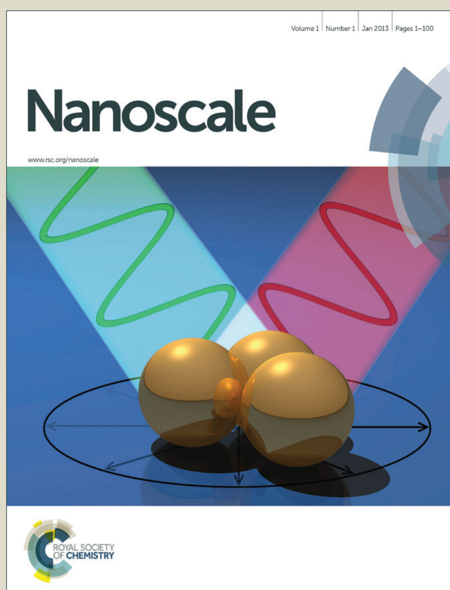

This is an *Accepted Manuscript*, which has been through the Royal Society of Chemistry peer review process and has been accepted for publication.

Accepted Manuscripts are published online shortly after acceptance, before technical editing, formatting and proof reading. Using this free service, authors can make their results available to the community, in citable form, before we publish the edited article. We will replace this *Accepted Manuscript* with the edited and formatted *Advance Article* as soon as it is available.

You can find more information about *Accepted Manuscripts* in the Information for Authors.

Please note that technical editing may introduce minor changes to the text and/or graphics, which may alter content. The journal's standard Terms & Conditions and the Ethical guidelines still apply. In no event shall the Royal Society of Chemistry be held responsible for any errors or omissions in this *Accepted Manuscript* or any consequences arising from the use of any information it contains.

ROYAL SOCIETY OF CHEMISTRY

www.rsc.org/nanoscale

Nanoscale RSCPublishing

ARTICLE

Robust Ag Nanoplate Ink for Flexible Electronics Packaging

Cite this: DOI: 10.1039/x0xx00000x

Ruo-Zhou Li,[a,b,c] Anming Hu,[b*] Denzel Bridges,[b] Tong Zhang,[a,c*] Ken D. Oakes,[d] Rui Peng,[e] Uma Tumuluri,[e] Zili Wu,[e] and Zhili Feng,[f]

Received 00th January 2012,
Accepted 00th January 2012

DOI: 10.1039/x0xx00000x

www.rsc.org/

Nanoinks are currently a topic of heightened interest with respect to low temperature bonding processes and printable electronics. We have developed an innovative polyvinylpyrrolidone (PVP)-stabilized Ag nanoplate ink amenable to very strong low temperature packaging, and investigated the relationship between bonding strength and electrical conductivity post-bonding. PVP shell plastic deformations observed in failure microcracks with the formation of PVP nanofibers, revealed bonding strength at low temperatures (<250 ℃) was primarily due to adhesive bonding. It is found that, utilizing photonic sintering, ~70℃ reduction of transformation temperature from adhesive to metallic bonding was achieved compared to that of thermal sintering. A numerical simulation was developed to better understand the influences of the light-induced heat generation, which demonstrated near-infrared light can facilitate sintering. Bonding strengths of 27 MPa were achieved at room temperatures, and 29.4 MPa at 210℃ with photonic sintering. Moreover, the anisotropic resistivity was observed with different thermal dependences. These results demonstrate Ag nanoplate inks have potential for low temperature 3D interconnections in lead-free microcircuits, flexible electronic packaging, and diverse sensing applications.

Introduction

During the past decade, flexible electronics (or flex circuits) have drawn increasing attention due to their many advantageous properties including lightweight, portable, highly bendable, and potentially foldable attributes.[1-5] Flexible electronics use solders to mount functional devices onto thermally-sensitive flexible organic substrates such as polyimide, or transparent conductive polyester films.[6, 7] One technical challenge is that these polymer substrates cannot maintain their function and stabilities above 200°C;[8] however, such high temperatures are required for melting conventional lead-free solders.[9, 10] Consequently, new solder materials and packaging protocols enabling low temperature bonding would be advantageous.

One approach to address the aforementioned issue exploits the "melting-point depression" phenomenon, whereby the melting point of a material is reduced by increasing surface energy as particle size decreases.[11-13] As a result, solid state sintering temperatures of nanomaterials are only 10-33% that of their bulk counterparts[14] facilitating the sintering of nanomaterials at low (< 200℃) temperatures. In light of these very low sintering temperatures, interest in sintering Ag nanoparticle inks for microelectronics packaging has been growing although typically these inks exhibit bonding strengths less than 12 MPa[11] and while Cu nanoparticle inks exhibit bonding strengths of around 13 MPa.[15] Peng et al. reported a room-temperature pressure less bonding process utilizing one-dimensional Ag nanowires instead of sphere nanoparticles, revealing that the particle shape can affect sintering and thereby the ultimate bonding.[16] Recent research efforts have focused on both sintering nanoplates and understanding shape effects, where required sintering temperatures are influenced by nanoparticle shape. Shape is critical as a molecular dynamics simulation demonstrated that atoms at the vertex of a triangular nanoplate possess a higher diffusion rate than interior atoms, allowing these triangular nanoplates to self-sinter and form nanobelts at room temperature with a growth-oriented capping agent.[14, 17] Such room temperature sintering, as a recent work reported, may facilitate the use of Ag nanoplates as conductive media for inkjet printing. Lee et al. reported the use of Ag nanoplates as inkjet ink particles instead of sphere Ag nanoparticle could improve conductivity and reduce post-processing temperature.[18] Nevertheless, to the best of our knowledge, there have been few studies on Ag nanoplates focusing on flexible electronic packaging. The mechanical performance of Ag nanoplates for packaging remain unclear.

Recently, new sintering protocols in addition to thermal approaches have been developed such as electrical,[19, 20] chemical,[21] and pressure-assisted sintering[15]. Photonic sintering should prove advantageous as surface plasmon resonance is generated by high intensity light focussed at the gap between two adjacent metallic nanoobjects,[22, 23] producing localized heating. As this heat is highly concentrated on a small area, it is less damaging to the substrate.[22, 24] This sintering protocol may benefit the use of nanomaterials for bonding purposes.

In this paper, we describe using Ag nanoplates as the solder amenable to thermal and photonic sintering for low temperature

Nanoscale Accepted Manuscript

packaging, and investigate the relationship between bonding strength and electrical conductivity post-bonding. The anisotropic resistivity was observed. We further report plastic deformation of polyvinylpyrrolidone (PVP) shells surrounding Ag nanoplates in failure microcrack with the formation of PVP nanofibers, revealing their bonding strength was mainly due to adhesive bonding. However, we demonstrate a transformation from adhesive to metallic bonding at temperatures above 250℃ for thermal, but at 180℃ for photonic bonding; this result demonstrates enhanced strength and conductivity is possible at 60-70 ℃ lower sintering temperatures with light-assisted bonding. A numerical simulation was run to better understand the influences of the light-induced heat generation, which demonstrated near-infrared light can pass through Ag nanoplate layers to heat the deeper areas of Ag nanoplate inks. Finally, we demonstrated potential applications of Ag nanoplate inks in flexible circuitry, planar resistors, or as solders for 3 dimensional (3D) packaging.

Experimental

Materials

$AgNO_3$, NaCl, ethylene glycol (EG), reagent alcohol and PVP (average molecular weight (MW) ≈ 1,300,000, for Ag nanoplate synthesis) powder used for this study were purchased from Fisher Scientific International. PVP powder of average MW ≈ 40,000 (for Ag nanowire synthesis) was purchased from Sigma-Aldrich Corporation. All reagents were used without further purification.

Preparation of Ag nanoinks

Several one-step methods have been reported showing the feasibility of synthesis Ag nanoplates at a large scale.[25, 26] In our experiment, Ag nanoplates were synthesized in PVP solution by a modified one-pot hydrothermal method.[27] Such seed-free method with an enhanced Ag concentration or a batch-processing may provide a green, simple and scalable route for practical applications. During synthesis, 1 mL of 1 M aqueous AgNO3 solution was added into 9 mL of 3.33 M aqueous PVP solution of MW ≈ 1,300,000. The mixture was then autoclaved in a stainless steel reactor inside a 23 mL Teflon-lined container at 120℃ for 21 h, then naturally cooled to room temperature. Ag nanowires were compared in thermal and photonic sintering and synthesized by a wet chemical method[28] according to protocols described by Reference 24. After synthesis, the nanoinks were prepared by washing the Ag nanoplates and nanowire with de-ionized (DI) water to remove excess PVP and alternatively condensed 3 times by centrifugation.[24] Finally, the precipitated sediments were collected and dispersed in ultrapure water (electrical resistivity ~18 MΩ cm). No additional dispersant was need for the ink.

Bonding using Ag nanoinks

Copper wires (0.2 mm thick) were cut into 40 mm lengths and ultrasonically cleaned in acetone for 5 min, HCl (10%) for 2 min and rinsed in ultrapure water to remove surface organic contaminants and oxidation prior to bonding.[16] For thermal bonding, a pipette was used to drop-cast Ag nanoink into the joint of two clean copper wires. Then the samples were expose in flowing air to speed up the solvent evaporation. The post-annealing process includes a heating procedure use a hotplate which either remained at room-temperature (24℃) or was heated from 40℃ to 300℃ in air for 1 h at the absence of bonding pressure. For light-assisted bonding (i.e., photonic sintering - see experimental setup in Fig. S2a), a Xenon flash lamp (1200 W) or tungsten lamp (250 W) was used to illuminate the samples during both the drop-casting and post-annealing processe. When using the Xenon flash lamp, the flash tube maintained the lamp a consistent distance of 4 cm from the samples with a constant light intensity (0.17 W/cm^2) and frequency (10 Hz). A hotplate was used to heat the sample from 40℃ to 200℃. When using the tungsten lamp, the bulb was placed at varying distances from the samples to heat them from 40℃ to 200°C.

Measurements

The maximum failure force was measured using a force gauge and the tensile shear strength was estimated using $\sigma = F_{\max} / A$, where F_{max} is the maximum failure force, and A is the cross-sectional area.[16] The nanofiber-shape plastic deformations of PVP shells across the microgaps, formed during the tensile tests, were cut using a dual beam FIB/SEM instrument (Zeiss Auriga Crossbeam FIB/SEM) for TEM and SEM observation. Additional TEM and HRTEM observations were performed using a ZEISS LIBRA 200. Extinction spectra of the Ag nanoplate films were obtained with a UV-VIS Spectrophotometer. The thermogravimetric analysis (TGA) was carried out using a thermal analyser (TA Instruments Q500) with a heating rate of 10 ℃/min. FTIR spectroscopy was conducted using Nicolet Nexus 670 FTIR spectrometer. The resistivity of Ag nanoplate and nanowire films were calculated using $\rho = A \times R / l$, where resistance R was measured by a digital voltmeter (HP 3456A), A and l are the cross-sectional area and length respectively.

Results and discussion

Characterization of Ag nanoinks

Monodispersed Ag nanoplates, which comprised ~ 20% (w/w) of the nanoplate ink, were characterized by SEM to have an average diameter of ~ 170 nm and 17 nm thickness (Fig. 1a;

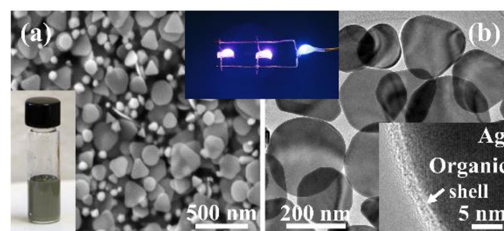

Fig. 1 (a) Typical SEM image of silver nanoplate ink (inset is the Ag nanoplate ink in a vial) (b) TEM images of Ag nanoplates (inset is a HRTEM image of an Ag nanoplate edge; PVP organic shell thickness is about 3nm). The top inset shows LEDs with Ni-coated copper wire bonded using Ag nanoplate inks.

Nanoscale Accepted Manuscript

Fig. S1a and b, Supplementary Information). The Ag nanowires, which comprised ~5% (w/w) of the nanowire paste were, on average, ~15 μm long and 60 nm thick with an average aspect ratio of 300 (Fig. S1c and S1d). Highly concentrated Ag nanoplate ink in a vial has a dark gray appearance (Fig. 1a), while the Ag nanowire ink is grayish yellow. Ag nanoplate detailed morphology can be seen by TEM image (Fig. 1b), as triangular and hexagonal nanoplates. Fig. S3 shows a HRTEM image of nanoplate recorded along the (111) plane of fcc Ag with 2.50 Å in spacing between lattice fringes. Typically, the as-prepared Ag nanoplates are capped by thin layers of PVP, which adsorbed onto the surface during the crystal growth of Ag nanoplates.[26] This is further confirmed by FTIR spectra (Fig. S4), which are in good agreement with earlier reports in literature.[29, 30] The absorption peaks at 1458 cm^{-1} and 1428 cm^{-1} are characteristic absorptions of the pyrrolidinyl group and the peaks at 1695 cm^{-1} and 1017 cm^{-1} can be attributed to the C=O and C–N vibrations in PVP, respectively.[29] These existing typical peaks evidence that Ag nanoplates are capped by PVP shells. The HRTEM image clearly illustrates the amorphous structure of PVP shell (Fig. 1b). During our synthesis, PVP served as the reducing agent, structure directing and surface capping reagent, and dispersant that kept the Ag nanoplates from aggregating and oxidizing.[15, 31] Nevertheless, the incorporation of metal nanoparticles into a polymer matrix such as PVP will impair nanoparticle sintering as a considerable fraction will form cross-linked polymer matrices.[21, 32] While previous studies reported the difficulty of de-bonding or decomposing the outer PVP shells, the shell thickness itself can be controlled during production by washing with deionized (DI) water and centrifugation.[16] In our experiments, the PVP shell thickness was approximately 3 nm following three washes. Notably, the washed Ag nanoplate ink can be stored at 7℃ for more than 6 months without loss of integrity, which is comparable to the useful life of Ag nanowire ink following two washings, and better than that of Ag nanowire inks with three washings.[16] Any precipitated sediment following storage can be re-dispersed by ultrasonication and stirring.

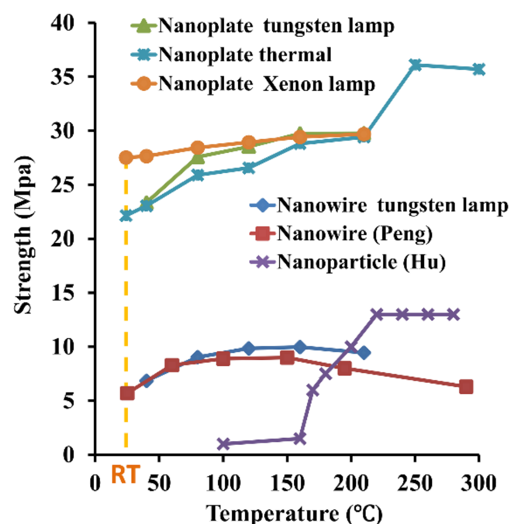

Fig. 2 Bonding strengths of Cu wires joined with Ag nanoplate ink as a function of bonding temperatures, with inks-post treated by Xenon flash or tungsten lamp compared (Ag nanowire ink data from Reference 15, Ag nanoparticle from Reference 11).

Thermal sintering

Joining performance of Ag nanoplate inks were investigated by joining two copper wires (Fig. S2b and c; Supplementary Information). The bonding strength of thermally sintered silver nanoplates (Fig. 2, light blue line) is notably three times higher than that of Ag nanowire inks at the same temperature[16] with bonding strengths gradually increase from 22.2 MPa at room temperature to 29.4 MPa at 210°C.

In contrast to Ag nanowire ink, whose maximum strength

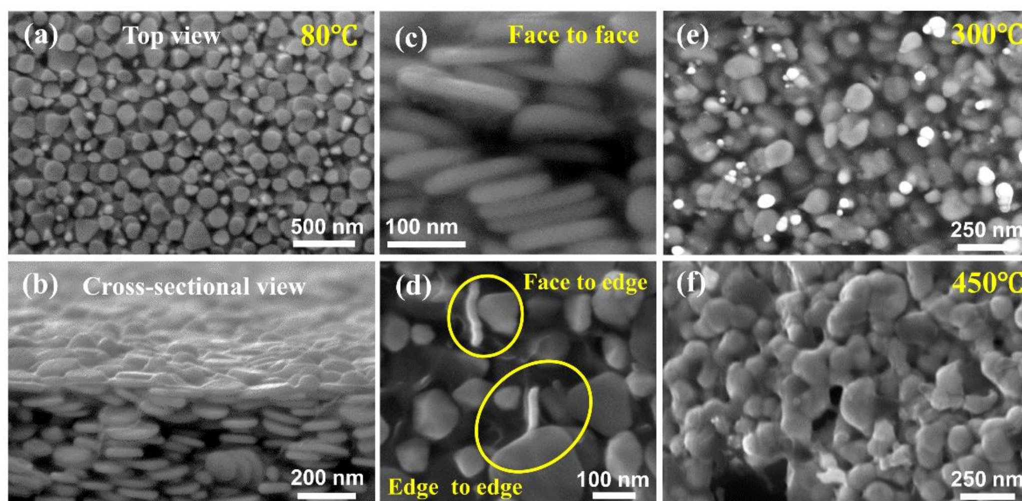

Fig. 3 SEM image of Ag nanoplate ink bonding at a temperature of (a) 80℃ (top view), (b) 80℃ (cross-sectional view), (c) 80℃ (nanoplates face to face), (d) 80℃ (nanoplates face to edge and edge to edge contact), (e) 300℃ (f) 450 ℃.

Nanoscale Accepted Manuscript

occurs at 150℃, the nanoplate ink rapidly increases in bonding strength from 210℃ to 250℃, stabilizing at roughly 36 MPa at 250℃, nearly 6 times higher than the Ag nanowire ink. The bonding strength of Ag nanoparticle ink (reported in Reference 11) shows similar bonding behavior at temperatures higher than 150 ℃, exhibiting a sharp rise in bonding strength due to sintering. Nevertheless, at temperatures below 160 ℃, Ag nanoparticle ink only displays bonding strengths around 1 MPa, considerably weaker than the silver nanoplate ink.

Compared with the reported results in which the bonding strength is mainly from the sintering among metallic nanoparticles or nanowires,[11, 15, 16, 33] although pure Ag nanoplates can sinter at room temperature, in the present work, the sinter was limited by PVP shells at a temperature below 250℃. Fig. 3a and b illustrate the top and cross-sectional views of the Ag nanoplate ink at a joint. Interestingly, Ag nanoplates tend to form an anisotropic laminated structures rather than the isotropic structures formed by Ag nanoparticles and nanowires (Fig. S3, Supplementary Information)[11] Fig. 3c and d showing the tight morphology of Ag nanoplate inks heated at 80℃ for 1 h. Ag nanoplates are most likely to stick together oriented face-to-face (Fig. 3c) with edge-to-face (Fig. 3d) or edge-to-edge contacts (Fig. 3d) being relatively rare. Such face-to-face contacts are similar as those reported in a literature, where the Ag nanoplates are separated by thin PVP shells.[34] Few obvious necks are formed at temperatures below 250℃, as Ag nanoplate sintering was limited by the highly cross-linked PVP polymer coating on the nanoplate surfaces.[16, 21] Fig S6 shows the TGA and DTG curves of Ag nanoplates and pure PVP heated in air. Except for the weight loss of PVP power was observed at a temperature below 100℃ due to the evaporation of absorbed water, no significant weight loss can be seen in both Ag nanoplates and PVP samples at a temperature below 250℃, indicating that no obvious decomposition of PVP in these temperature ranges. This is also confirmed by FTIR spectra shown in Fig S4 with minimized changes of characteristic peaks for both samples post-processed at room temperatures and 160 ℃. PVP, a widely used industrial adhesive commercially available in glue stick and hot-melt adhesives, contributes to the highly ordered interlaced and laminated structure and strong binding force with additional adhesive contributions. Hence, such interlaced and laminated Ag nanoplates slicked by capping PVP, contributes to the high bonding strength below 250℃.

The decomposition of PVP took place from 250℃as FTIR spectra indicates (shown in Fig S4). At this temperature, it could be seen a drop off, splitting and red-shift of the 1695 cm^{-1} peak attributed to C=O vibrations. Similarly, the 1458 cm^{-1} and 1428 cm^{-1} peaks due to pyrrolidinyl groups are also weakened. The decomposition of PVP shells of Ag nanoplates in air lead to two peaks (FigS6) (in DTG cures shown in FigS6), indicating the highest weight loss rate at temperatures around 350℃and 400℃, similar to those of pure PVP. Noteworthy, only the peak at 400℃ was observed when Ag nanoplates were heated in nitrogen, indicating the decomposition of PVP shells around 350℃ is due to the oxidation of PVP. Upon the decomposition of PVP, sintering of Ag nanoplates was observed with a conformational change from nanoplates to nanoparticles, with necks formed between adjacent nanoparticles (Fig. 3e). The bonding mechanism gradually transferred from adhesive bonding to metallic bonding at this temperature. At 450℃, the sintered Ag nanoplates form porous 3D Ag nano-networks (Fig. 3f).

The UV-vis spectra unveil the similar variation. The extinction spectrum as a function of bonding temperature (Fig. 4) of as-prepared Ag nanoplate film on a glass slide was similar to previous reports[35] with an in-plane dipole plasmon resonance peak at 890 nm. Typically, sintering of nanostructures leads to morphological changes, in turn affecting the surface plasmon resonance and absorbance spectra.[22] *In situ* observation of spectral changes during thermal processing revealed little intensity change from 24℃ to 160℃. A slight blue-shift in the main peak from 892 nm to 624 nm at 200℃ indicates that the Ag nanoplates became rounded.[30, 36] At 200℃, only a slight absorption decrease occurring at less than 280 nm was observed, demonstrating the existence of un-decomposed PVP. Most of the thermodynamic driving force available for sintering was inhibited at 200℃; at higher temperatures, the decomposition of PVP removed this inhibition, allowing for densification and sintering.[37] This process can be observed as the temperature is increased to 250℃ as the continuing absorption decrease from 215 nm to 280 nm, demonstrating the decomposition of PVP. A blue-shift of the main peak to 474 nm is similarly a consequence of sintering. Meanwhile, the intensity of the resonant peak weakens and broadens, indicating the forcmation of larger and more complex metallic structures (Fig. 3f). Collectively, these data demonstrate that the Ag nanoplate ink possesses largely adhesive bonding at temperatures below

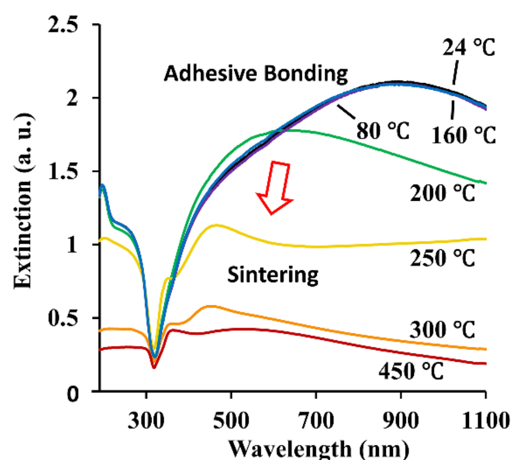

Fig. 4 UV-vis spectra of Ag nanoplate inks illustrating temperature-dependent bonding dominated by adhesive bonding <250℃, and solid state diffusion (sintering) processes above 250℃.

~250℃, shifting to dominantly solid state diffusion bonding (sintering) at temperatures above 250℃ (Fig. 4).

Photonic sintering

Nanoscale Accepted Manuscript

To further increase bonding strength, we employed a Xenon flash lamp to illuminate the samples with a fixed light intensity during the drop casting and post-heating processes. Incident light energy at the SPR (Surface Plasmon resonance) wavelength is extremely localized within the ultra-small volume between two Ag nanoplates due to the strong plasmon coupling effect.[23] Thus, similar to Ag nanowires, heat generation is naturally self-contained at the junction point,[22] in other words, heat generation is very localized, decreasing markedly with distance from the joint. As shown previously, Ag nanoplate dimmers possess a narrow-band resonance spectrum (in the tens of nanometers range) with peak intensity and position dependent on the surrounding media, gap distance and morphology of the adjacent Ag nanoplate inks (SNPs).[23] The Ag nanoplate inks in our work exhibit a 600 nm FWHM (full width at half maximum) broad-band light absorption owning to diverse sizes, multiple morphologies and the random distribution of Ag nanoplates. This broad absorption band spanning 500 nm to 1100 nm matches the Xenon flash emission spectrum which has been extensively used by the printable electronics industry. The orange top line in Fig. 2 illustrates Ag nanoplate ink sintered by Xenon flash, a process which yielded an additional 5 MPa of bonding strength at room temperature. This bonding strength improvement produced by photonic sintering gradually disappears with increasing temperatures, demonstrating the dominant role of metallic bonding under these conditions.

Xenon flash sintering of Ag nanoplate inks at 180 ℃ generates morphologies with two (Fig. 5a-c) and three (Fig. 5d) nanoplates bonded, illustrating the transformation from adhesive bonding to dominantly metallic bonding with the assistance of light. Notably, Xenon flash illumination enables this transformation at 180℃; ~70℃ lower than the processing temperature required for thermal bonding.

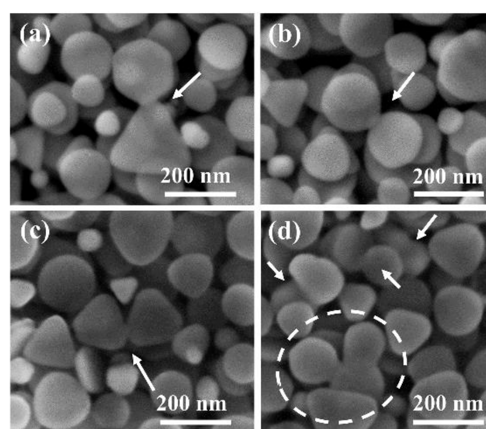

Fig. 5 SEM image of Ag nanoplate ink bonding by Xenon flash light at a temperature of 180℃. Joints between Ag nanoplates with (a) hexagonal and triangular shapes, (b) two round nanoplates, and (c) two triangular nanoplates, and (d) 3 nanoplates as indicated by arrows.

To further elucidate the effect of light on bonding strength, a tungsten lamp was used to illuminate and heat the sample at increasing distances, which was inversely correlated with sample surface temperature. As expected, the differential bonding strength between the lamp and thermal sintering (the triangular and cross symbols, Fig. 2 upper lines) initially increased to a maximum of approximately 2 MPa, then

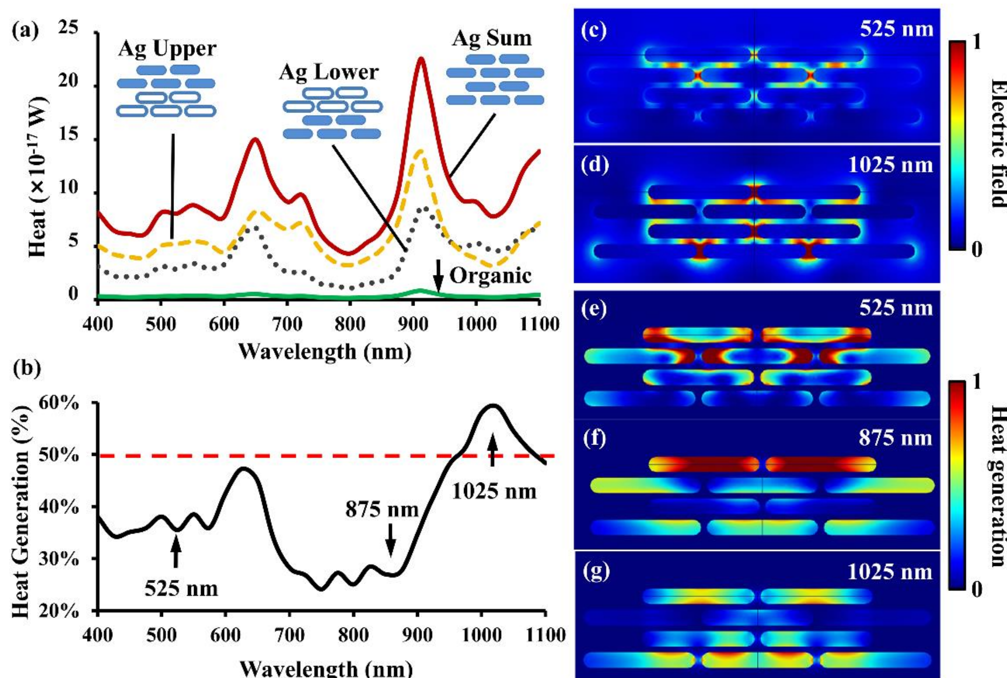

Fig. 6 (a) Calculated heat generated as a function of wavelength in four Ag nanoplate layers. The dashed line represents heat generated in the upper two layers of Ag nanoplates, the dotted line represents heat generated in the lower two layers, while the solid line marked "Ag Sum" is the total heat generated in all four silver nanoplate layers. The line labelled "organic" is the heat generated in the PVP matrix. (b) Percentage of heat generated in the upper two layers relative to all four layers. Electric field distribution at wavelengths of (c) 525 nm and (d) 1025 nm. Heat distribution at wavelengths of (e) 525 nm, (f) 875 nm and (g) 1025 nm.

Nanoscale Accepted Manuscript

decreased with increasing temperatures. Similar experiments, using Ag nanowire rather than nanoplate ink, were also conducted (Fig. 2). Photonic sintering of Ag nanowires[22, 24] also yielded an improvement in bonding strength, demonstrating the universal potential of photonic sintering to strengthen bonds at lower temperatures than achievable by thermal sintering.

Heat generation in Ag nanoplate inks via light absorption

To better understand heat generation during photonic sintering, we modelled heat generation in Ag nanoplates using a 3D simulation based on a Finite Element Method (FEM).[23] To simplify, we considered an ideal conduction scenario with 4 layers of laminated Ag nanoplates immersed in PVP with un-polarized incident light (plane wave with a wide band ranging from 400 nm to 1100 nm and a light intensity of 1 W/m^2) vertically illuminating the Ag nanoplates. The complex refractive indices of silver and PVP were analytically fit using experimental data[38, 39] with Fig. 6a demonstrating heat generation by layer and as a function of wavelength. First, when comparing heat generation in Ag nanoplates and in the organic PVP layer, clearly most heat is generated in Ag rather than PVP due to the much higher absorbance of Ag. Although light is concentrated in the PVP nanogaps between Ag nanoplates (Fig. 6c and 6d), the heat generated in Ag remains two orders of magnitude greater than that generated in PVP, which is essentially negligible (Fig. 6e-g). Notably, the heat generated near the edge of Ag nanoplates of the surface layer is at a shorter wavelength (as shown in Fig. 6e); if it was at a longer wavelength, such heat would be less localized in the nanoplates. However, due to the high thermal conductivity of Ag, heat generated at the edge or other "hot spots" can rapidly spread to the whole Ag nanoplate.[40]

At wavelengths shorter than 950 nm, relatively more heat is generated in the surface layers, but longer wavelengths can penetrate through to deeper layers (Fig. 6d), as evidenced by the percentage of heat generated in the lower 2 layers (Fig. 6b). Heat generated in the upper 2 layers (yellow dashed line) is about twice that generated in the lower 2 layers (black dotted line) at a wavelengths shorter than 950 nm (Fig. 6a). In contrast, at wavelengths between 950 nm and 1100 nm, more heat is generated in the lower layers, demonstrating near infrared light in this region can propagate deeper into the lower Ag nanoplate ink layers via SPR to generate deeper heat, demonstrating the significance of the Xeon flash lamp infrared band for photonic sintering.

Plastic deformation of PVP shells

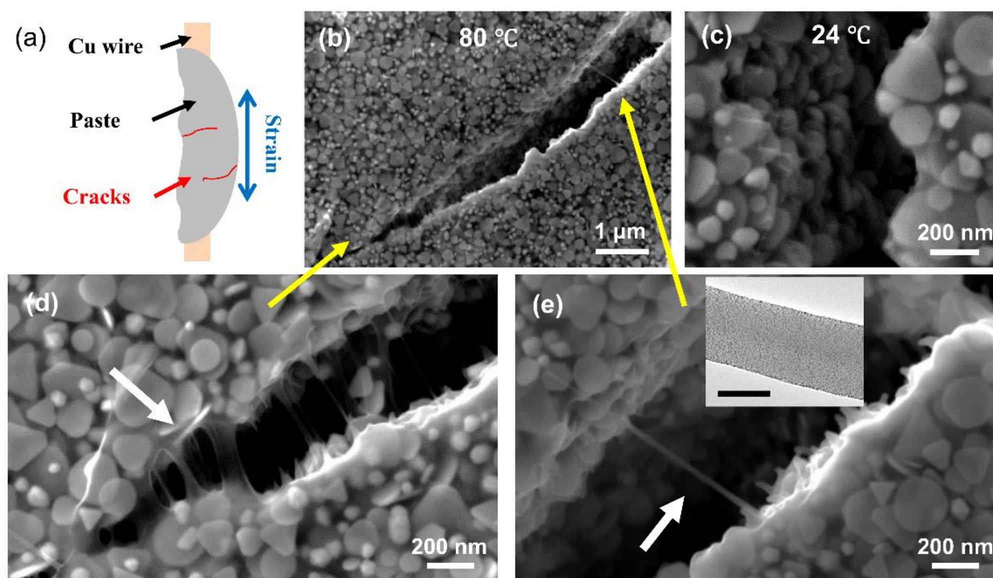

Fig. 7 (a) Schematic illustration of microcracks formed during tensile testing. Microcracks in Ag nanoinks post-processing (b) posted heating at 80℃ for 1 h and (c) in room temperature (24℃) without post-heating (d) High magnification SEM image of glue-style plastic deformation of PVP shells, (e) a nanowire shaped plastic deformation; arrows indicate deformation site. Inset is a HRTEM image of the organic PVP nanowire. The black scale bar indicates 50 nm.

Nanoscale Accepted Manuscript

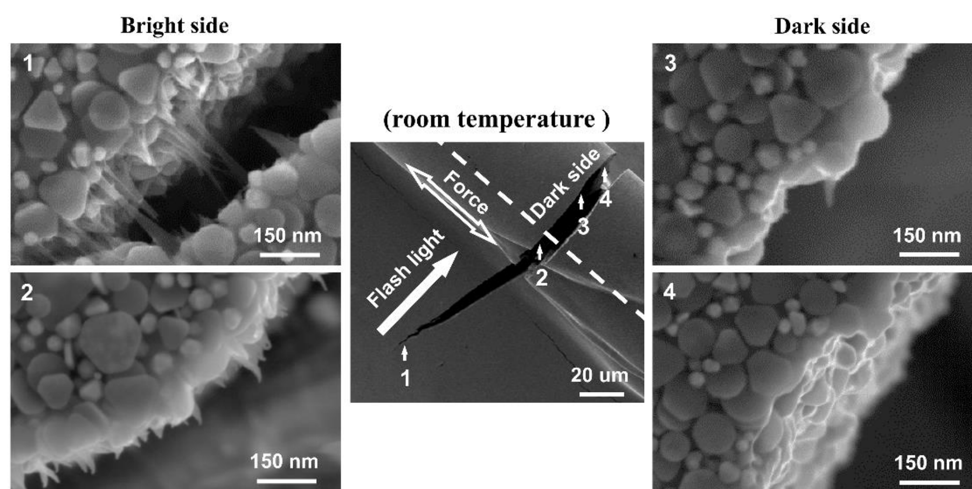

Fig. 8 SEM image of silver nanoink illuminated by a Xenon flash on only one side (bright side). Images 1-4 are high magnifications of plastic deformations and microcracks at the sites marked in the center low magnification SEM image.

To further investigate adhesive bonding fracture mechanisms in Ag nanoplate inks, fracture surfaces were examined by SEM. During tensile testing, in addition to the filler fracture parallel to the strain along the copper wires, a few micro-cracks perpendicular to the strain were observed (Fig. 7a). These regions reveal the role of the PVP shell in the Ag nanoplate ink fracturing as the primary crack cannot be readily characterized after failure.[41] At room temperature, few deformations can be found in the gap (Fig. 7c), but as the bonding temperature increases, glue-style plastic deformations in the micro-cracks can be observed (Fig 7b). In enlarged images of Fig. 7b, sample heated at 80 ℃ reveals plastic deformations of the micro-crack form nanofibers of several micrometers in length, and tens of nanometers in thickness (Fig. 7d and 7e). Notably, HRTEM images (inset in Fig. 7e and S4a, see Supplementary Information) and Energy-dispersive spectroscopy (Fig. S4b, Supplementary Information) indicate that these nanofibers are amorphous PVP.

These microcrack organic plastic deformations reveal the failure of Ag nanoplate ink processed at temperatures below 250 ℃ occurring in the PVP shell. The formation of these plastic deformations at this temperature is probably based on adjacent Ag nanoplates being joined primarily by their PVP shells, which during failure were partially drawn away from the Ag nanoplates, as indicated by the arrow in Fig. 7d. After "drawing-out" these organic PVP nanofibers, they are now susceptible to final failure, forming glue-style plastic deformations. Again, this supports the hypothesis that the bonding of Ag nanoplate inks processed below 250 ℃ are mainly due to adhesion of their PVP outer shells, rather than the Ag nanoplates themselves.

To further explore the effect of light-induced localized heating on plastic deformation, a room temperature experiment was conducted using a Xenon flash to illuminate the sample from one side only (bright side) while the other side (dark side) received no illumination (Fig. 8). A microcrack crossing the bright side to the dark side exhibited an almost clear separation lacking plastic deformations, while the bright side possessed glue-style plastic deformations similar to those observed upon heating to 80 ℃. Based on these deformations results, local

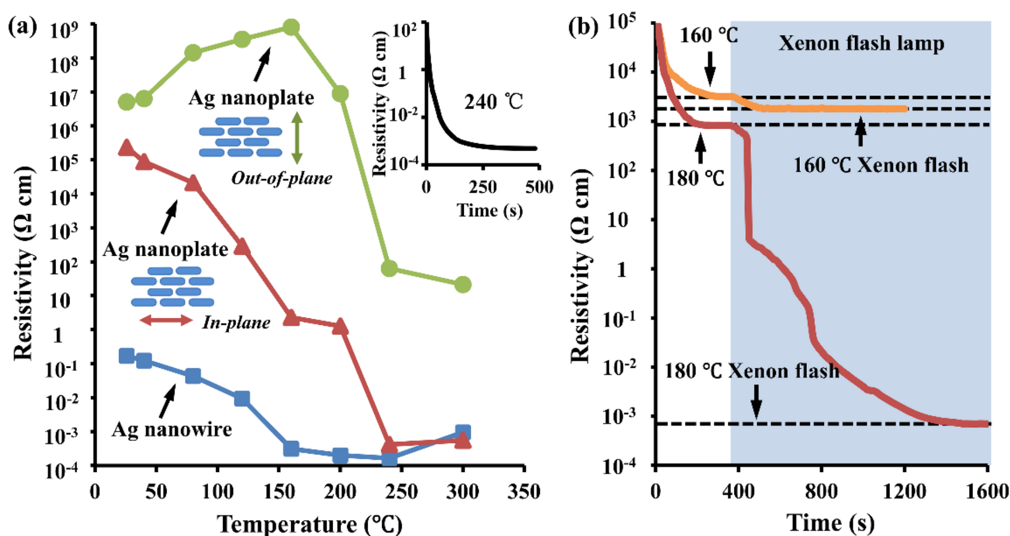

Fig. 9 (a) The resistivity of Ag nanoplate and nanowire ink as a function of bonding temperature. (b) The resistance of silver nanoplate ink on glass substrate as a function of time; shaded region indicates the period of ink illumination

Nanoscale Accepted Manuscript

heating associated with photonic sintering probably cross-linked PVP shells to as the main source of adhesive bonding strength.

Electrical properties of Ag nanoplate inks

To quantitatively analyze the sintering process, we monitored the change in electrical resistance throughout the sintering process (Fig. 9a). Ag NWs begin to sinter even at room temperature, with resistance decreasing as temperature increases. At temperatures around 150℃, solid state diffusion (sintering) of silver atoms allows the building of metallurgic bonds while further reducing electrical resistance.[22, 42] Compared with Ag nanowires with isotropic structures, as we mentioned, Ag nanoplates tend to form an anisotropic laminated structures, leading to anisotropic resistivity: in-plane resistivity and out-of-plane resistivity as shown in Fig. 9a. Both in-plane and out-of-plane resistivity of Ag nanoplates is 6-7 orders of magnitude higher than Ag nanowires at room temperature; this high resistivity is partially attributable to the limited sintering of Ag nanoplates compared with nanowires, but also the steric structure and unique shape of silver nanoplates which can limit physical contact at room temperature. The different thermal behaviors of in-plane and out-of-plane resistivity may be attributed to different PVP thicknesses and vaporization/decomposition rates in two directions.

Interestingly, reverse variations of in-plane and out-of-plane resistivity was observed from room temperature to 160℃. In contrast of in-plane resistivity, the out-of-plane resistivity shows around 2 order of magnitudes increase of resistance while the in-plane resistivity shows 5 order magnitudes decrease of resistance. This results in a resistivity difference increasing from 2 orders in room temperature to 9 orders at 160℃. The unusual resistivity behaviors may be a consequence of anisotropic sintering. Our previous molecular dynamic simulation (MD) study shows the in-plane sintering is thermally preferable.

As temperature further increases, the PVP shell partially decomposes which increases contact points between adjacent Ag nanoplates to reduce resistivity;[37, 43] however, increased nanoplate contact produced by the densification of the silver nanoplate filler in a polymer matrix (influenced by solvent (water) vaporization) is likely the dominant factor improving conductivity. At 240 ℃, both in-plane and out-of-plane resistivity decreases quickly within 5 min, then stabilizes at a reistivity around 10^{-3} Ω cm and 10^{2} Ω cm, respectively. This decrease in resistance may reveal material transformation to a state which facilitates filament style channels based on solid state diffusion from the initial composite material which forced electrical hopping internally.[16, 19] Between 240℃ to 300℃, the increase in Ag nanowire ink resistivity is mainly due to broken nanowires[16] while at the same temperatures only a slightly increase of in-plane resistivity of Ag nanoplate ink was observed, likely due to oxidation. Again, Ag nanoplate inks demonstrate superior thermal stability than Ag nanowire inks.

Flash illumination from the Xenon lamp can dramatically influence electrically conductivity (Fig. 9b). The measurement carried out with an in-plane direction. At 160 ℃, when illuminated with a high intensity flash, only a minor change in resistance resulted, and this resistance remained relatively stable over time at quite high values of about 3000 Ω cm. However, with a small temperature increase to 180℃, a rapid decline in electrical resistance was observed. Consequently, photonic sintering greatly enhanced conductivity while reducing the required thermal threshold by approximately 60℃ relative to thermal bonding, which is of benefit if light-based sintering was integrated into roll-to-roll printing processes to facilitate cost-effective large-scale production.

Fig. 10a is an image of a circuit printed on flexible indium tin oxide (ITO)-coated polyethylene terephthalate (PET) substrate with 3D packaging. The circuit consists of Ag nanowire electrodes, an Ag nanoplate planar resistor, a light-emitting diode (LED) with two copper pins bonded to Ag nanowire electrodes with Ag nanoplate ink and a silver nanoplate connector through a blind via connecting the ITO (Fig. 10b). The blind via (0.2 mm diameter) was punched with a focused laser beam. Voltage applied to the Ag nanowire electrode propagates through the resistor, LED, moving through the blind via and completing the circuit through the ITO, thus lighting the LED. The circuit can be bent (Fig. 10c) demonstrating the feasibility of 3D packaging of electrical elements on a flexible substrate using Ag nanoplate and nanowire inks.

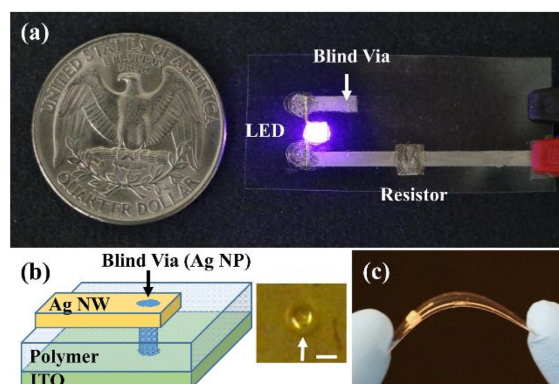

Fig. 10 (a) Flexible circuit printed on ITO substrate consisting of Ag nanowire electrodes, an Ag nanoplate planar resistor, a LED with two copper pins bonding to nanowire electrodes using Ag nanoplate ink, and a silver nanoplate blind via cascading the Ag nanowire electrodes from the obverse side to the ITO on the back side. (b) Schematic diagram of the blind via connecting the Ag nanowire (Ag NW) electrode and the ITO film. Inset is the top-down optical image of a blind via, white scale bar indicates 200 μm. (c) Circuit flexibility demonstrated in profile.

Conclusions

Nanoscale Accepted Manuscript

Silver nanoplate inks have been developed through PVP-assisted hydrothermal synthesis capable of bonding Cu wires. Shear strengths can reach 22 MPa at room temperature due to the adhesive bonding of PVP shells, and 36 MPa at 250℃ due to metallurgic bonding based on solid state diffusion sintering of silver nanoplates. Room temperature bonding strengths are enhanced to 27 MPa by illuminating with intensive flash light. Simulated light propagation through textured silver nanoplate layers revealed infrared light penetrated to deeper layers of silver nanoplate ink, modifying conductivity. Also, the anisotropic resistivity was observed with different thermal dependences. These differences are discussed in the framework of anisotropic sintering of nanoplates and thermal vaporization and decomposition of PVP capping layers. Finally, construction of a small, flexible, yet functional circuit demonstrated the feasibility of silver nanoplate inks for numerous potential applications including wearable electronics on flexible and stretchable substrates.

Acknowledgements

We appreciate the research initiative funding provided by the University of Tennessee as a new hire package to AH. Part of the work including the thermal analysis and FTIR was conducted at the Center for Nanophase Materials Sciences, which is a DOE Office of Science User Facility. This work is also in part supported by NSFC under grant number 61307066, Doctoral Fund of Ministry of Education of China under grant number 20110092110016 and 20130092120024, Natural Science Foundation of Jiangsu Province under grant number BK20130630, the National Basic Research Program of China (973 Program) under grant number 2011CB302004 and the Foundation of Key Laboratory of Micro-Inertial Instrument and Advanced Navigation Technology, Ministry of Education, China under grant number 201204, a strategic research project (KZ40005001) of the Education Commission. We also appreciate Dr John R Dunlap for the assistance in FIB sample preparation and TEM (JIAM Analytical Instrument Facilities, University of Tennessee at Knoxville).

Notes

[a] School of Electronic Science and Engineering, Southeast University, Key Laboratory of Micro-Inertial Instrument and Advanced Navigation Technology, Ministry of Education, Nanjing 210096, China.

[b] Department of Mechanical, Aerospace, & Biomedical Engineering, University of Tennessee, Knoxville 37996, USA.

[c] Suzhou Key Laboratory of Metal Nano-Optoelectronic Technology, Suzhou Research Institute of Southeast University, Suzhou 215123, China.

[d] Verschuren Centre, Department of Biology, Cape Breton University, P.O. Box 5300, 1250 Grand Lake Rd., Sydney, B1P 6L2 Canada.

[e] Center for Nanophase Materials Sciences and Chemical Science Division, Oak Ridge National Laboratory, P.O. Box 2008, Oak Ridge, TN 37831-6493.

[f] Materials Processing and Joining, Materials Science and Technology Division Oak Ridge National Laboratory, P.O. Box 2008, Oak Ridge, TN 37831-6083.

† Electronic Supplementary Information (ESI) available: this section includes size distributions of silver nanoplate and nanowire, schematic illustration of wire configuration during bonding, HRTEM image of an Ag nanoplate, FTIR spectra and thermal analysis of Ag nanoplates. SEM image of sintered Ag nanowire ink, and TEM and EDS image of a PVP nanofiber. See DOI: 10.1039/b000000x/

References

1 D. Tobjork and R. Osterbacka, *Adv Mater*, 2011, **23**, 1935-1961.
2 M. Koo, K.-I. Park, S. H. Lee, M. Suh, D. Y. Jeon, J. W. Choi, K. Kang and K. J. Lee, *Nano letters*, 2012, **12**, 4810-4816.
3 Y. Zhang, C. Lei and W. S. Kim, *Appl Phys Lett*, 2013, **103**, 073304.
4 G.-W. Huang, H.-M. Xiao and S.-Y. Fu, *Nanoscale*, 2014, **6**, 8495-8502.
5 S. H. Chae, W. J. Yu, J. J. Bae, D. L. Duong, D. Perello, H. Y. Jeong, Q. H. Ta, T. H. Ly, Q. A. Vu and M. Yun, *Nature materials*, 2013, **12**, 403-409.
6 X. Liu, M. Mwangi, X. Li, M. O'Brien and G. M. Whitesides, *Lab on a Chip*, 2011, **11**, 2189-2196.
7 U. Zschieschang, T. Yamamoto, K. Takimiya, H. Kuwabara, M. Ikeda, T. Sekitani, T. Someya and H. Klauk, *Advanced Materials*, 2011, **23**, 654-658.
8 Y. Lu, J. Y. Huang, C. Wang, S. Sun and J. Lou, *Nature nanotechnology*, 2010, **5**, 218-224.
9 I. Mir and D. Kumar, *Int J Adhes Adhes*, 2008, **28**, 362-371.
10 C.-A. Lu, P. Lin, H.-C. Lin and S.-F. Wang, *Jpn J Appl Phys*, 2007, **46**, 4179.
11 A. Hu, J. Y. Guo, H. Alarifi, G. Patane, Y. Zhou, G. Compagnini and C. X. Xu, *Appl Phys Lett*, 2010, **97**, 153117.
12 C. Yang, C. P. Wong and M. M. Yuen, *Journal of Materials Chemistry C*, 2013, **1**, 4052-4069.
13 E. Marzbanrad, A. Hu, B. Zhao and Y. Zhou, *The Journal of Physical Chemistry C*, 2013, **117**, 16665-16676.
14 E. C. Neyts and A. Bogaerts, *The Journal of Physical Chemistry C*, 2009, **113**, 2771-2776.
15 Y. Jianfeng, Z. Guisheng, H. Anming and Y. N. Zhou, *J Mater Chem*, 2011, **21**, 15981.
16 P. Peng, A. Hu, H. Huang, A. P. Gerlich, B. Zhao and Y. N. Zhou, *J Mater Chem*, 2012, **22**, 12997.
17 B. M. Amoli, E. Marzbanrad, A. Hu, Y. N. Zhou and B. Zhao, *Macromol Mater Eng*, 2014, **299**, 739-747.
18 C.-L. Lee, K.-C. Chang and C.-M. Syu, *Colloids and Surfaces A: Physicochemical and Engineering Aspects*, 2011, **381**, 85-91.
19 A. Vafaei, A. Hu and I. A. Goldthorpe, *Nano-Micro Letters*, 2014, **6**, 293-300.
20 Y. Mei, Y. Cao, G. Chen, X. Li, G.-Q. Lu and X. Chen, *Device and Materials Reliability, IEEE Transactions on*, 2013, **13**, 258-265.
21 S. Magdassi, M. Grouchko, O. Berezin and A. Kamyshny, *ACS nano*, 2010, **4**, 1943-1948.
22 E. C. Garnett, W. Cai, J. J. Cha, F. Mahmood, S. T. Connor, M. G. Christoforo, Y. Cui, M. D. McGehee and M. L. Brongersma, *Nature materials*, 2012, **11**, 241-249.
23 X.-Y. Zhang, A. Hu, T. Zhang, W. Lei, X.-J. Xue, Y. Zhou and W. W. Duley, *ACS nano*, 2011, **5**, 9082-9092.
24 R. Z. Li, A. Hu, T. Zhang and K. D. Oakes, *ACS applied materials & interfaces*, 2014, **6**, 21721-21729.

Nanoscale Accepted Manuscript

25 X. Liu, L. Li, Y. Yang, Y. Yin and C. Gao, *Nanoscale*, 2014, **6**, 4513-4516.
26 I. Washio, Y. Xiong, Y. Yin and Y. Xia, *Advanced Materials*, 2006, **18**, 1745-1749.
27 L.-Z. Ren and J.-X. Wang, *Frontiers of Materials Science in China*, 2010, **4**, 407-410.
28 T. Zhang, Y.-J. Song, X.-Y. Zhang and J.-Y. Wu, *Sensors*, 2014, **14**, 5860-5889.
29 H. Liu, B. Zhang, H. Shi, Y. Tang, K. Jiao and X. Fu, *J Mater Chem*, 2008, **18**, 2573-2580.
30 B. Tang, S. Xu, X. Hou, J. Li, L. Sun, W. Xu and X. Wang, *ACS applied materials & interfaces*, 2013, **5**, 646-653.
31 I. Washio, Y. Xiong, Y. Yin and Y. Xia, *Advanced Materials*, 2006, **18**, 1745-1749.
32 R. Zhang, K.-s. Moon, W. Lin and C. Wong, *J Mater Chem*, 2010, **20**, 2018-2023.
33 J. Yan, G. Zou, A. Wu, J. Ren, A. Hu and Y. N. Zhou, *J Electron Mater*, 2012, **41**, 1886-1892.
34 G. S. Métraux and C. A. Mirkin, *Advanced Materials*, 2005, **17**, 412-415.
35 R. Jin, Y. Cao, C. A. Mirkin, K. Kelly, G. C. Schatz and J. Zheng, *Science*, 2001, **294**, 1901-1903.
36 B. Tang, J. An, X. Zheng, S. Xu, D. Li, J. Zhou, B. Zhao and W. Xu, *The Journal of Physical Chemistry C*, 2008, **112**, 18361-18367.
37 J. G. Bai, T. G. Lei, J. N. Calata and G.-Q. Lu, *J Mater Res*, 2007, **22**, 3494-3500.
38 E. D. Palik, *Handbook of optical constants of solids*, Academic press, 1998.
39 H. H. Hakim, A.; Abdul-Hafidh, G.; Alyaa, H. A.; Mohammed, S. , *European Scientific Journal* 2013, **9**, 132-137.
40 G. Baffou, R. Quidant and C. Girard, *Appl Phys Lett*, 2009, **94**, 153109.
41 P. Peng, A. Hu, B. Zhao, A. P. Gerlich and Y. N. Zhou, *J Mater Sci*, 2012, **47**, 6801-6811.
42 J. Sommer and C. Herzig, *J Appl Phys*, 1992, **72**, 2758-2766.
43 D. Untereker, S. Lyu, J. Schley, G. Martinez and L. Lohstreter, *ACS applied materials & interfaces*, 2009, **1**, 97-101.

Nanoscale Accepted Manuscript